

X-RAY DIFFRACTION CHARACTERIZATION OF THE RESIDUAL STRESS AND HARDNESS DISTRIBUTIONS IN INDUCTION HARDENED GEARS

Douglas J. Hornbach, Paul S. Prev y, and Perry W. Mason
Lambda Research

ABSTRACT

Accurate knowledge of the subsurface residual stress and hardness distributions is required for failure analysis, fatigue life prediction and process control of induction hardened components. X-ray diffraction (XRD) provides a powerful tool for the simultaneous determination of both the macroscopic residual stress and hardness distributions through the case and into the core of induction hardened parts. A procedure for developing the empirical relationship between diffraction peak width and mechanical hardness is described.

Subsurface XRD residual stress measurement requires layer removal and correction for the resulting stress relaxation. The corrections may dominate the results obtained at depths near the case/core interface. Traditional closed-form corrections may be inadequate when applied to gear teeth. A novel finite element analysis (FEA) correction technique applicable to arbitrary geometries and stress distributions is presented and described. Examples of the determination of the residual stress and hardness distributions through the case of induction hardened gears are presented.

INTRODUCTION

Hardening of steel requires heating the steel to a temperature above its austenitic transformation point followed by quenching at a rate faster than the critical cooling rate. The critical rate depends upon the chemistry of the alloy. Following the quenching operation the steel should contain a hard martensitic phase which will form only in the thin case of carburized or induction hardened parts. The swelling that occurs during the martensitic phase transformation

will generally produce a compressive residual stress distribution in the case. Compressive residual stresses at the surface can increase fatigue life and decrease the likelihood of failure under high applied stresses. However, residual stresses produced by hardening depend upon the component geometry, and can vary greatly in magnitude or even become tensile under certain combinations of hardening parameters and geometry, degrading component life.

In the induction hardening process a surface layer is heated using a high frequency power supply and shaped coil. The temperature distribution and depth of the heated layer can be controlled by varying the frequency, time, and coil geometry. Following heating, the component is quenched in either air or liquid medium. Because the heating coils can be shaped to vary the area heated, induction hardening lends itself to components which require localized hardening or irregular geometries. Efficient use of material can be achieved by hardening localized areas of a component. A precise case depth can also be achieved with the induction hardening process, and induction heating offers higher energy fluxes than furnace carburizing.

Gears are frequently induction hardened. Because induction hardening produces minimal distortion, the gears can generally be completely machined in the soft state and then hardened in the final stages of manufacture. Wear of gear cutting tools and the time needed for machining the gears are therefore reduced. Induction hardenable carbon steels can often be used in place of more expensive higher alloy steels.

The induction hardening process must be optimized and controlled in order to achieve favorable hardness and residual stress distributions and the desired case depths. Once the residual stresses, hardness and case

depths produced by variations of the hardening parameters are quantified, the optimal induction hardening parameters can be achieved for a given material and component geometry.

X-ray diffraction techniques can be used to quantify the residual stresses⁽¹⁻⁴⁾ and hardness in cold worked or heat treated⁽⁵⁾ materials. The residual stress and hardness can be measured simultaneously at the surface and at any predetermined depths below the surface by electropolishing material for subsurface measurement. Measurements can be made at depth increments as small as 2.5 μ m (0.0001 in.) using continuously variable irradiated areas as small as 0.5 mm, providing depth and spatial resolution exceeding all other methods of residual stress measurement. A hardness profile can be determined at fine increments through the case/core interface or in any region or depths of interest employing high resolution x-ray diffraction techniques and an appropriate combination of electropolishing and precise sample positioning.

The objective of this study was to quantify the residual stresses and hardness in the case and core of induction hardened gears through the use of x-ray diffraction techniques. The x-ray diffraction residual stress data were corrected for stress relaxation caused by material removal in the complex geometry of a gear tooth using finite element techniques. The subsurface hardness distributions through the case were derived from the width of the diffraction peak used for residual stress measurement.

SPECIMEN DESCRIPTION

Three induction hardened SAE six-pitch 1552 steel test gears were supplied by Contour Hardening. The geometry of the gear, developed under sponsorship of the Gear Research Institute, is shown in Figure 1. The gears were identified by serial numbers 61, 63, and 65.

The gears had an outside diameter of nominally 152.4 mm (6.0 in.), an inside diameter of 38.1 mm (1.5 in.), a maximum bore width of 50.8 mm (2.0 in.), and a tooth length of nominally 25.4 mm (1.0 in.).

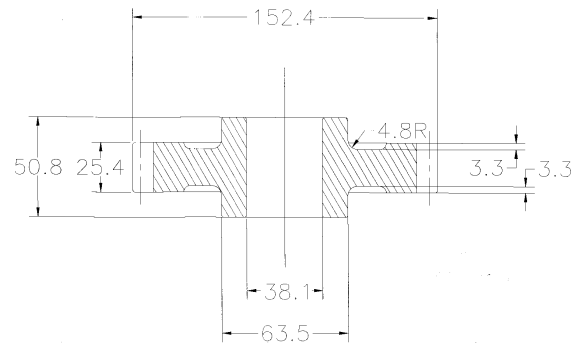


Fig. 1 SAE Six-Pitch test gear dimensions (in mm). 143.9 mm pitch diameter is indicated.

The induction hardening parameters, varied for the three samples, were the time of preheat and the dwell time before the final heat. The values of the varied parameters are listed in the table below.

Gear Serial Number	Time of Preheat (sec.)	Dwell Before Final (sec.)
61	7.0	10.00
63	4.85	1.35
65	6.50	5.00

The Time of Preheat and Dwell Before Final columns indicate the amount of time, in seconds, during which the power supply was on during preheat and off prior to the final heating, respectively. The parameters which were held constant for all three gears are listed below:

Preheat Parameters	Final Heat Parameters	Time of Final Heat (sec.)	Time of Quench (sec.)
150 kW, 10 kHz	300 kW, 300 kHz	0.5	8.0

MEASUREMENT PROCEDURE

X-RAY DIFFRACTION RESIDUAL STRESS MEASUREMENT

X-ray diffraction was used to measure the residual stresses and the hardness due to the induction hardening process of the gear specimens S/N 61, 63 and 65. The XRD measurements were taken at mid-length of an arbitrary gear tooth at a distance of nominally 0.5 mm (0.020 in.) from the edge of the root radius, nominally 7.1 mm (0.279 in.) from the crown of

the tooth, as shown in Figure 2.

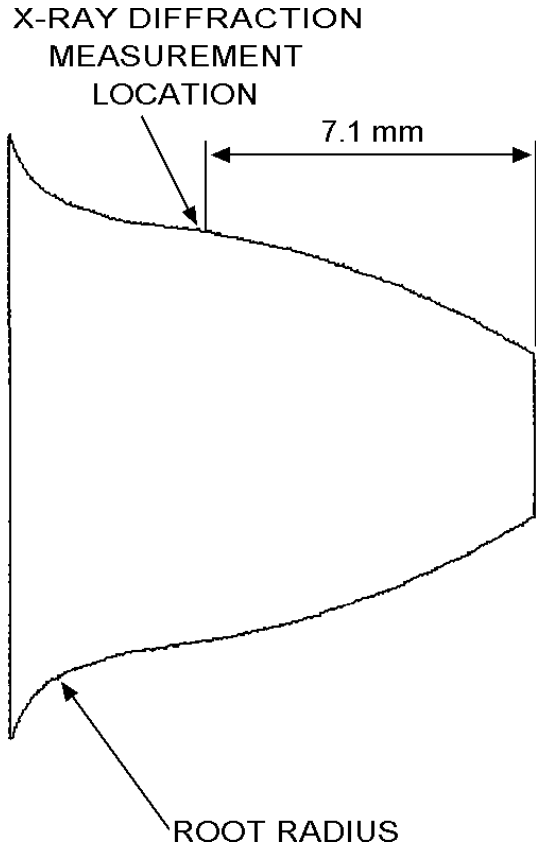


Fig. 2 Location of x-ray diffraction measurement on tooth pitch-line.

X-ray diffraction residual stress measurements were initially performed using a $\sin^2\psi$ technique employing the diffraction of chromium radiation from the (211) planes of the BCC crystal structure of 1552 steel. The measurement was performed at the surface of S/N 61. The multi-angle $\sin^2\psi$ technique was performed to determine whether or not the lattice spacing was a linear function of $\sin^2\psi$ as required for the plane-stress linear elastic macroscopic residual stress model. The (211) diffraction peak angular positions were determined for positive ψ tilts of 0, 18.4, 26.6, 33.2, 39.2, and 45.0 deg.

Because the lattice spacing was found to be a linear function of $\sin^2\psi$, as required for the plane-stress model, the majority of the x-ray diffraction residual stress measurements were performed using a two-angle $\sin^2\psi$ technique, in accordance with SAE J784a. The diffraction peak angular positions at each of the ψ tilts employed for measurement were determined from the position of the $K\alpha_1$ diffraction peak separated from the

superimposed $K\alpha$ doublet assuming a Pearson VII function diffraction peak profile in the high back-reflection region⁽⁶⁾. The diffracted intensity, peak breadth, and position of the $K\alpha_1$ diffraction peak were determined by fitting the Pearson VII function peak profile by least squares regression after correction for the Lorentz polarization and absorption effects, and for a linearly sloping background intensity.

Details of the diffractometer fixturing are outlined below:

Incident Beam Divergence:	0.2 deg.
Detector:	Scintillation set for 90% acceptance of the Chromium $K\alpha$ energy
ψ Rotation:	10-50 deg.
Irradiated Area:	1.0 x 5.0 mm (0.04 x 0.20 in.) (short axis in the radial direction)

The value of the x-ray elastic constant, $E/(1 + \nu)$, required to calculate the macroscopic residual stress from the strain measured normal to the (211) planes of SAE 1536 steel was previously determined empirically⁽⁷⁾ employing a simple rectangular beam manufactured from SAE 1536 steel loaded in four-point bending on the diffractometer to known stress levels and measuring the resulting change in the spacing of the (211) planes in accordance with ASTM E1426-91.

Material was removed by electropolishing for subsurface measurement, minimizing possible alteration of the subsurface residual stress distribution as a result of material removal. All data obtained as a function of depth were corrected for the effects of the penetration of the radiation employed for residual stress measurement into the subsurface stress gradient.⁽⁸⁾

STRAIN GAGE STRESS RELOCATION MONITORING

Sectioning of the gear samples was necessary prior to the x-ray diffraction residual stress measurement in order to provide access for the incident and diffracted x-ray beams. Rather than cutting away adjacent teeth, teeth were removed from the gear to provide multiple tooth samples. As part of the procedure, strain gage rosettes were applied at the location at which the x-ray diffraction measurements were to be made. A single TMP FRA-1-11-1L strain gage was applied on each

tooth at mid-length so the center of the grids were nominally 0.5 mm (0.020 in.) from the point of tangency with the root radius. The strain relaxation due to removing each gear tooth was monitored and recorded. The stress relaxation was then calculated assuming isotropic material and plane stress on the surface. The calculated sectioning stress relaxations were used to correct the x-ray data for relaxation which occurred as each tooth was removed for measurement. The sectioning stress relaxation which occurred beneath the surface was assumed to be equal to that which was measured on the surface.

FINITE ELEMENT CORRECTION FOR LAYER REMOVAL

The x-ray diffraction residual stress measurements were corrected for stress relaxation as a result of removing material by electropolishing. As stressed layers of material were removed, the remaining stresses in the body and on the exposed surface were altered. Due to the relatively complex geometry of the gear tooth, the relaxation as a function of material removal could not be easily solved by available closed-form solutions developed for flat plates and cylinders with symmetrical residual stress distributions⁽⁹⁾. Therefore, a three dimensional finite element model, shown in Figure 3, employing over 2000 first order isotropic hexahedral elements was built to determine the relaxation that occurred in the body as the stressed layers were removed after XRD measurement. A linear finite element model was built, assuming that during relaxation, the material behaved elastically as a result of material removal. Because the tooth was removed from the gear prior to electropolishing, the boundary conditions were assigned so the tooth was free to relax in any direction.

Artificial thermal loads were employed to simulate the residual stresses in the model. The strain needed to produce the residual stress measured in the top layer of elements was achieved by varying the temperature. The stress re-equilibration throughout the subsurface elements due to the stressed top layer of elements could then be determined. The stress relaxation, which occurred in subsurface elements due to subsequent removal of overlying stressed layers, was integrated over the number of stressed layers removed. Following removal of all of the layers, a model containing a simulated electropolished pocket, as shown in Figure 3, was achieved.

A flat plate with an arbitrary stress distribution was modeled prior to studying the stress relaxation due to material removal in the more complex gear tooth. Two and three dimensional flat plate models were studied to compare the relaxations due to layer, strip, and pocket material removal geometries. These results were compared to the closed-form solutions for uniform layer removal of flat plates⁽⁹⁾. The plate had dimensions of 101 mm (4 in.) square by 25.4 mm (1.0 in.) thick. The FEA models were artificially thermally loaded to a depth of 3.05 mm (0.120 in.) to give a near constant compressive stress distribution with a magnitude on the order of -400 MPa (-60 ksi). The layer, strip, and pocket were then removed at increments of nominally 500 μm (0.02 in.) and the stresses which were relaxed below the removed layer were calculated.

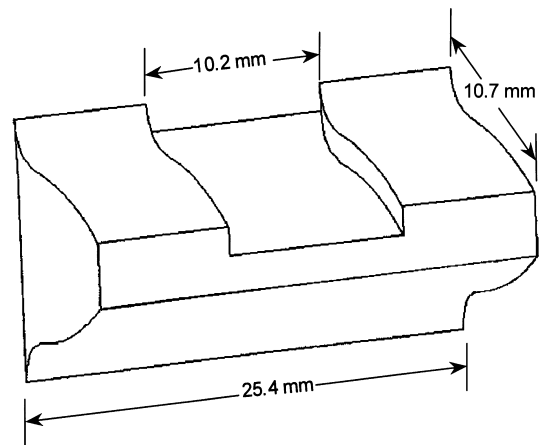


Fig. 3 Nominal dimensions of layer removal zone used in finite element modeling.

HARDNESS DETERMINATION

To relate the peak widths to the hardness, a tooth from the gear was removed and tempered at nominally 300 C at 15 min. time intervals to reduce the hardness from full hardness down to material softer than the gear core. The hardness at the surface of the tooth was mechanically measured on the Rockwell C scale at each tempering interval. The full width at half height of the (211) $K\alpha_1$ diffraction peak of the surface material was also determined by multiple x-ray diffraction measurements at each tempering interval using Pearson VII function peak profile plotting.⁽⁶⁾ An empirical curve relating the (211) diffraction peak width to the HRC hardness for 1552 steel was created by plotting the peak width vs. the hardness as shown in Figure 4.

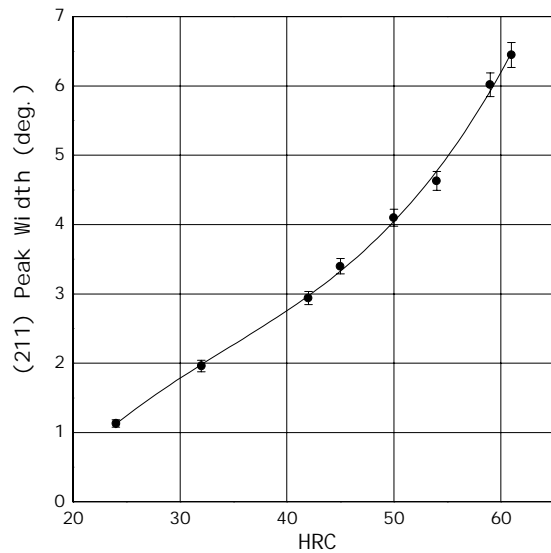


Fig. 4 Dependence of (211) peak width on Rockwell C hardness. Cubic polynomial fit shown.

Microhardness testing was performed on each gear tooth using a Leco M-400-G1 hardness tester following the ASTM E384 specification. A Vickers indenter was used with a 500 gram load. This setup allowed the hardness to be determined at a minimum depth increment of nominally $51 \mu\text{m}$ (0.002 in.).

RESULTS

FINITE ELEMENT MODEL

The FEA results of the flat plate stress relaxations, due to various types of removals, are shown in Figure 5. The results indicated the pocket removal has the least affect on the stress relaxation in the material below the pocket. The removal of a band or strip of material from the face of the gear tooth produces the highest change in stresses, possibly due to an increase in the stress intensity due to the formation of the slot. The FEA and closed-form analytical solutions⁽⁹⁾ for uniform layer removal are in good agreement.

The FEA calculation of stress relaxation which occurred during layer removal in each gear tooth are shown in Figure 6. The FEA results are plotted against a correction calculated from closed-form solutions for full layer removal for a flat plate⁽⁹⁾ of the same thickness as the gear tooth at the location of XRD stress measurement.

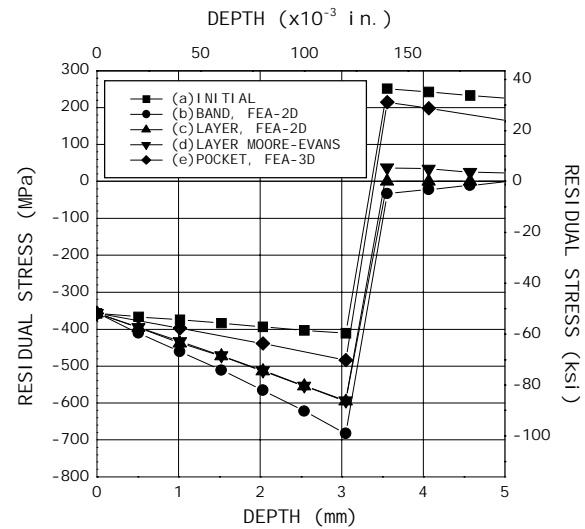


Fig. 5 Comparison of relaxation of simulated stress distribution as a result of various layer removal methods in a flat plate.

- (a) Initial linear stress distribution.
- (b) FEA solution of band perpendicular to stress.
- (c) FEA full layer.
- (d) Moore and Evans full layer removal.
- (e) FEA pocket, three dimensional.

The actual relaxation revealed by the FEA solution is seen to be over twice the magnitude of the correction calculated for a flat plate of uniform thickness, and is a function of the stress distribution in the part. The FEA results shown in Figure 6 were applied to the XRD measured residual stresses to correct for stress relaxation in the gear teeth.

X-RAY DATA

The multi-angle $\sin^2 \psi$ data, shown in Figure 7, indicate a linear relationship between $\sin^2 \psi$ and the lattice spacing. The $F(\psi)$ function, the normalized (211) peak intensity, indicates relatively uniform intensities across the range of ψ tilts examined. These data indicate a well behaved fine grained steel without significant preferred orientation.

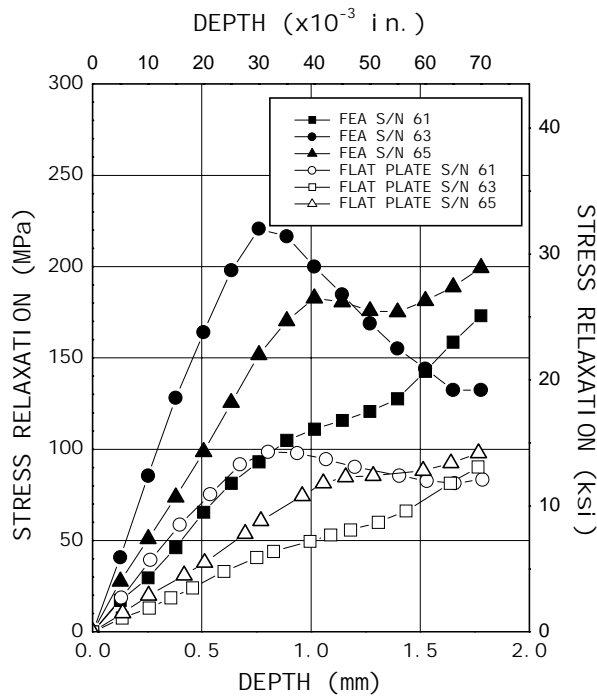


Fig. 6 Comparison of three dimensional pocket and Moore and Evans corrections applied to test data showing under correction by flat plate approximation.

The radial residual stress distributions measured as functions of depth are shown in Figures 8 through 10. The results indicate compression near the surface of all three specimens. The data for specimen S/N 63, hardened with the shortest preheat and dwell time of 1.35 sec., show the highest compression of all three gears near the surface, reaching -500 MPa at a depth of nominally 200 μ m. Note that Figure 9 is plotted on an expanded scale. The results for gear S/N 61 indicate that the longest preheat and dwell times produced the lowest magnitude compressive stresses, reaching only nominally -150 MPa and exhibiting complex oscillations in the stress distribution. The results show a trend of increasing compression as a function of decreasing dwell and preheat times.

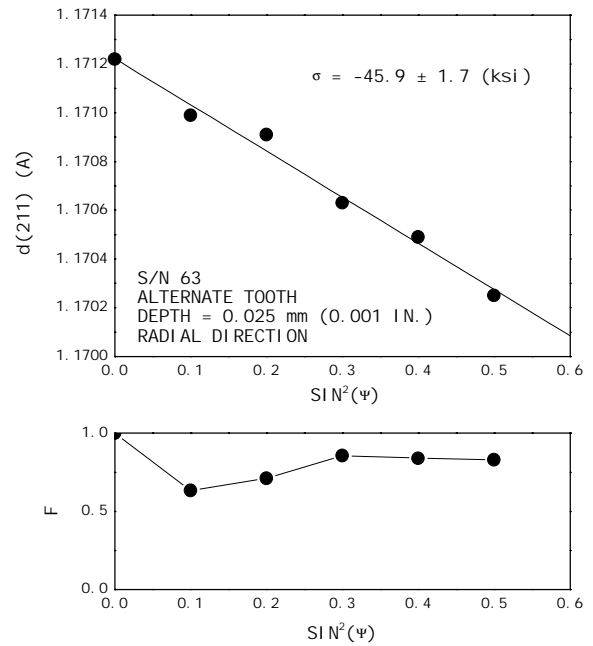


Fig. 7 Lattice spacing vs. $\text{Sin}^2(\psi)$ on alternate tooth, S/N 63, showing linear dependence of $\text{Sin}^2(\psi)$ and uncertainty.

A shorter dwell time will tend to harden a shallower depth of material given that the material has less time to conduct heat. Upon quenching, this relatively shallow layer of material seems to produce higher compression than a deeper layer of material which has been heated for a longer period of time producing a more uniform temperature. The depth of the compressive layer also appears to be a function of the dwell time. Again, the shorter dwell times will produce a shallower layer of heated material and, therefore, a shallower layer of compression is achieved.

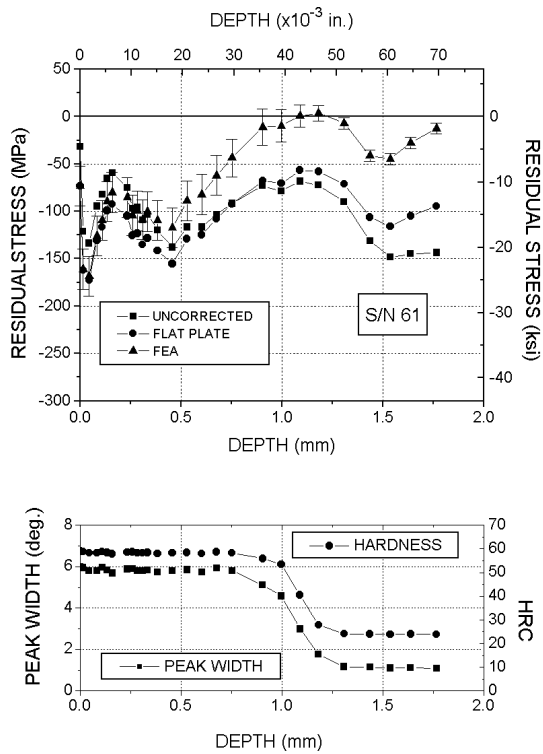


Fig. 8 Subsurface residual stress, hardness and peak width distributions for specimen S/N 61 comparing layer removal correction methods.

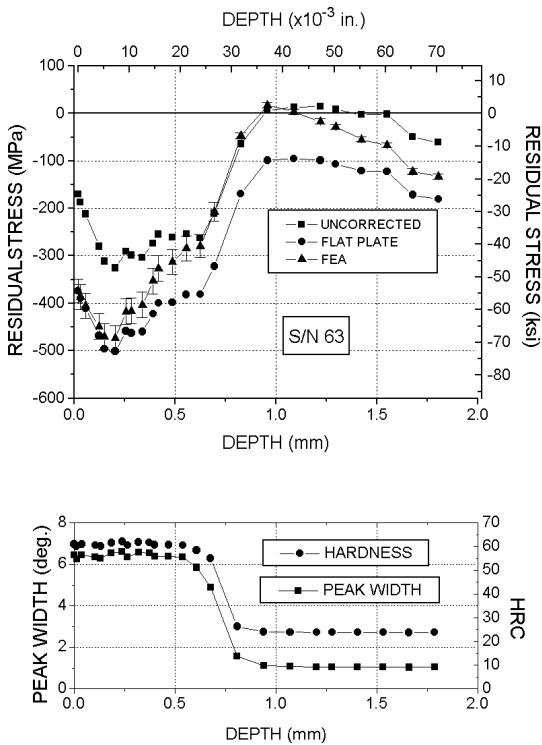


Fig. 9 Subsurface residual stress, hardness and peak width distributions for specimen S/N 63 comparing layer removal correction methods.

correction methods.

The oscillations observed in the residual stress distributions shown in Figure 8, and to a lesser degree in Figure 10 for specimens 61 and 65, are occasionally observed in induction hardened components. In contrast, carburizing, in which the carbon potential is developed by diffusion of carbon into the steel, typically produces smooth monotonically decreasing compression as a function of depth, with the possible exception of reduced compression caused by surface decarburization. The oscillations seen in these data are attributed to the more complex variations of temperature distributions and cooling rates which can be produced by induction hardening. The greater variability possible by induction hardening provides greater versatility of application, but demands close monitoring of the stress and hardness distributions achieved.

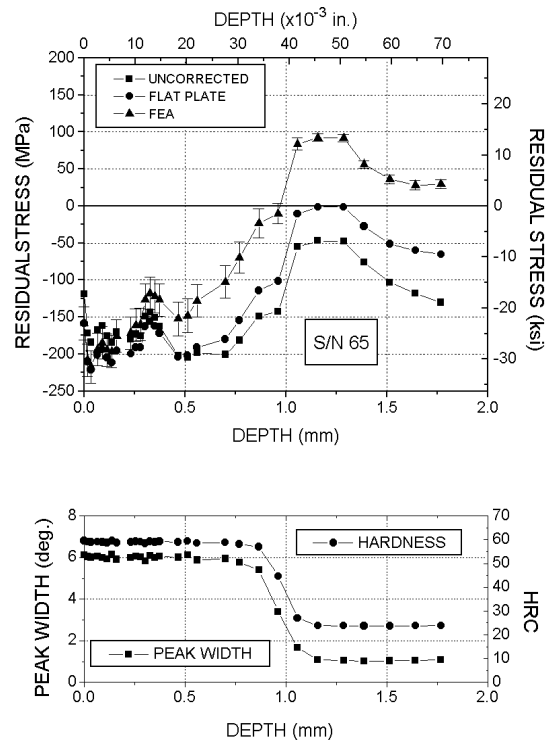


Fig. 10 Subsurface residual stress, hardness and peak width distributions for specimen S/N 65 comparing layer removal correction methods.

The peak width distributions and the corresponding hardness calculated as functions of depth are shown at the bottom of Figures 8 through 10. The results indicate a slightly harder case for gear S/N 63, over 60 HRC, relative to other two specimens, which are on the

order of 58 HRC. The increased hardness, again, may be a function of dwell time. The depth of the hardened material is shallower for the lower dwell times.

The XRD hardness data determined from the diffraction peak widths are compared with the mechanical microhardness data in Figures 11 through 13. The mechanical and XRD distributions are in good agreement. The data obtained mechanically do not define the decrease in hardness between the case and the core very well, lacking the depth resolution achieved with the shallow penetration of the x-ray beam.

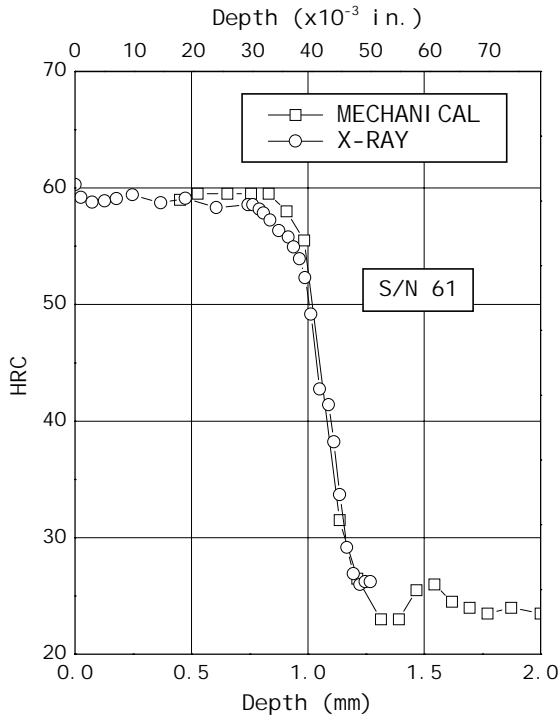


Fig. 11 Comparison of mechanical and x-ray subsurface hardness distributions for specimen S/N 61.

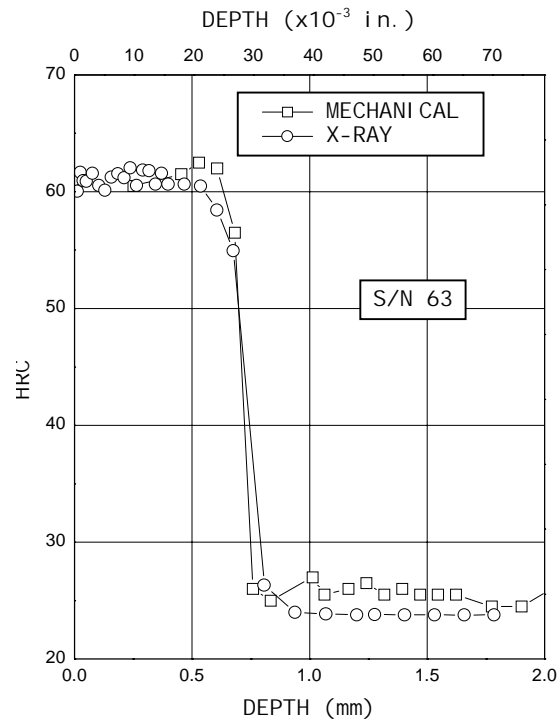


Fig. 12 Comparison of mechanical and x-ray subsurface hardness distributions for specimen S/N 63.

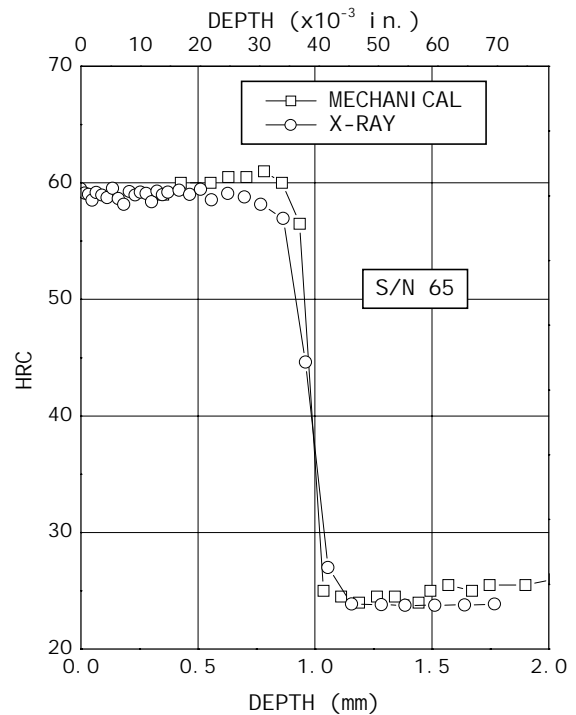


Fig. 13 Comparison of mechanical and x-ray subsurface hardness distributions for specimen S/N 65.

CONCLUSIONS

X-ray diffraction residual stress and line broadening measurement has been demonstrated to be a powerful tool for characterizing the complex residual stress and hardness distributions which can be produced by induction hardening of gear teeth. Several specific features of the x-ray diffraction technique demonstrated by this study are:

- 1) XRD provides the high depth and spatial resolution necessary to characterize the complex distributions of residual stress which can be produced by induction hardening.
- 2) XRD line broadening analysis can provide accuracy at least comparable to mechanical hardness determinations with superior depth resolution useful for characterizing the steep hardness gradients at the case/core interface of induction hardened gears.
- 3) A three dimensional finite element solution is necessary for accurate determination of the residual stress relaxation caused by layer removal for x-ray diffraction residual stress measurement in complex geometries. The magnitude of the relaxation cannot be ignored, and is a complex function of the gear geometry and stress distributions present.

Application of XRD residual stress and hardness determination using the FEA based relaxation corrections revealed several trends in the residual stress and hardness distributions developed in the SAE six-pitch 1552 steel test gears as a result of varying the preheat and dwell times:

- 1) The shorter preheat and dwell times produced higher magnitude compression in a shallower layer.
- 2) Shorter preheat and dwell times resulted in slightly higher case hardness.
- 3) The shallower, more compressive harder case produced by the shortest preheat and dwell times also produced a steeper hardness gradient between the case and core material.

ACKNOWLEDGEMENTS

The mechanical microhardness measurements were performed by Kathryn Evans of Metcut Research Associates. The gear samples and the induction hardening were provided by John Storm of Contour Hardening. The assistance and discussions with both contributors are greatly appreciated.

REFERENCES

1. Cullity, B. D., Elements of X-ray Diffraction, 2nd ed., Addison-Wesley, Reading, Massachusetts, 1978, pp. 447-476.
2. Hilley, M.E., ed., Residual Stress Measurement by X-Ray Diffraction, SAE J784a, Society of Automotive Engineers, 2nd ed., 1971.
3. Noyan, I. C. and Cohen, J. B., Residual Stress: Measurement by Diffraction and Interpretation, Springer-Verlag, New York, 1987.
4. Prev y, P. S., "X-Ray Diffraction Residual Stress Techniques," Metals Handbook, Vol. 10, American Society for Metals, Metals Park, OH, 1986, pp. 380-392.
5. Prev y, P. S., "The Measurement of Subsurface Residual Stress and Cold Work Distributions in Nickel Base Alloys," Residual Stress in Design, Process and Material Selection, American Society for Metals, Metals Park, OH, 1987, Young, William B., ed., pp. 11-19.
6. Prev y, P. S., "The Use of Pearson VII Distribution Functions in X-ray Diffraction Residual Stress Measurement," Advances in X-ray Analysis, Plenum, New York, Vol. 29, 1986, pp. 103-112.
7. Prev y, P. S., "A Method of Determining the Elastic Properties of Alloys in Selected Crystallographic Directions for X-ray Diffraction Residual Stress Measurement," Advances in X-ray Analysis, Plenum, New York, Vol. 20, 1977, pp. 345-354.
8. Koistinen, D. P. and Marburger, R. E., "A Simplified Procedure for Calculating Peak Position in X-ray Residual Stress Measurements on Hardened Steel," Transactions of the ASM, Vol. 51, 1959, pp. 537-550.
9. Moore, M. G. and Evans, W. P., "Mathematical Correction for Stress in Removed Layers in X-Ray Diffraction Residual Stress Analysis," SAE Transactions, Vol. 66, 1958, pp. 340-345.